Surface structures of approximant phases in the Al-Pd-Mn system

V. Fournée,* A. R. Ross, T. A. Lograsso, J. W. Anderegg, C. Dong,† M. Kramer, I. R. Fisher,** P. C. Canfield, and P. A. Thiel‡

Ames Laboratory, Departments of Materials Science and Engineering, Physics and Astronomy, and Chemistry, Iowa State University, Ames, Iowa 50011

(Received 8 April 2002; Submitted to Physical Review B April 2002; published 29 October 2002)

We present a study of the surface of the ξ'-Al-Pd-Mn approximant phase based upon scanning tunneling microscopy and low-energy electron diffraction. Several structures are observed on two different samples grown either by the Bridgman technique or by a self-flux method, and which contain various degrees of disorder. We also describe some other complex crystalline phases that are sometimes observed on the fivefold surface of Al-Pd-Mn quasicrystalline samples after the sputter-annealing cleaning process under ultrahigh vacuum conditions. This includes the *T* approximant phase resulting from surface decomposition after a high-temperature annealing.

DOI: 10.1103/PhysRevB.66.165423 PACS number(s): 61.44.Br, 68.35.Bs

I. INTRODUCTION

Quasicrystals (QC's) are aperiodic intermetallic alloys that possess a long-range positional order, with coherence length that can reach the micron scale.[1–3] They often exhibit crystallographically forbidden symmetries, most commonly fivefold and tenfold. The composition domain in which they form is usually limited to a small region in the phase diagram. This is due to a constraint imposed by the average number of valence electrons per atom (e/a) related to an electronic stabilization mechanism.[4]

In the neighborhood of this precise chemical composition, one often finds periodic structures with giant unit cells and a local atomic order that is very similar to the local order found in the QC. These alloys are called *approximant* phases as they are intrinsically related to their parent quasicrystal. More precisely, and in the framework of the cut method, the structures of a QC and its approximants can be derived from the same periodic object in a hyperspace of dimension $N > 3$.[5] Depending on the relative orientation of the three-dimensional (3D) physical subspace embedded in the hyperspace, the same *N*-dimensional periodic object will lead to either a quasiperiodic structure or a periodic approximant, via the cut and projection method.

So far, surface studies of this class of materials mainly revolve around a few quasicrystalline systems for which single grains can be prepared.[6] Besides the physical properties of technological relevance usually associated with these materials[7]—like low friction, reduced adhesion and high hardness—surface studies are motivated by fundamental interest in understanding how the complex atomic structure and the associated physical properties are modified at the 2D surface truncation.[8] In particular, what is the influence of the atomic clusters usually considered as the building blocks of the 3D structure of both QC's and their approximants? For QC's this actually depends on the way the surface has been prepared in the ultrahigh vacuum (UHV) chamber, the main options being fracture vs cycles of sputtering and annealing.

Scanning tunneling microscopy (STM) experiments have been carried out on several QC's, mostly on high-symmetry surfaces of the Al-Pd-Mn icosahedral phase. A rough and corrugated surface is observed when it is prepared by fracture.[9] It is believed that this results from a special stability of the cluster units that force the fracture plane to circumvent the clusters. On the other hand, when the same fivefold surface is prepared by cycles of sputtering and annealing, a terrace and step morphology is observed.[10–13] Both the three step heights measured (2.4, 4.1, and 6.5 Å) and the fine structure observed on the terraces are fully consistent with a bulk-terminated surface. Motifs with fivefold or tenfold symmetry appear in the high-resolution STM images, corresponding to cross sections through the 3D clusters of the bulk.

These recent results on quasicrystalline surfaces raise questions about the relative stability of the atomic clusters, since different preparation methods result in different surface topographies. It is clear that during sputtering by energetic Ar^+ ions (from 0.5 to 2 keV), the ion energy is sufficient to break apart the clusters and produce disorder in the top layers. Sputtering also shifts the composition away from the stability range of the icosahedral phase due to preferential sputtering of Al.[14] Annealing at sufficiently high temperature is therefore necessary to restore both the composition and the quasiperiodic order. And, it is interesting to note that the formation of flat terraces corresponding to specific dense layers is favored during this surface restoration rather than formation of the rough array of clusters that would (presumably) mimic the fracturelike surface.

In this paper, we explore the surface structure of various approximant phases, which are also cluster-based materials, both by STM and low-energy electron diffraction (LEED). We point out some key differences when they are compared with the surface of the parent icosahedral QC. The Al-Pd-Mn ternary system is a particularly interesting one as it contains, in addition to the stable icosahedral QC, a metastable decagonal QC and also various approximant phases with close chemical composition, both on the Mn-rich side (the *T* and *R* approximants) and on the Pd-rich side (the ξ' and ξ approximants) of the phase diagram.[15] In the following section, we give experimental details about the single crystals of the ξ' approximant samples used in this study, which were produced by two different growth techniques. Then we present

results concerning their surface structure perpendicular to the pseudo-tenfold axis. One sample appears to contain a higher density of structural defects than the other. We also describe some observations of other complex crystalline phases resulting from a surface transformation of an icosahedral $Al_{72}Pd_{19.5}Mn_{8.5}$ quasicrystalline sample. The preparation process in UHV induces this transformation. The complex crystalline phases are the *T* approximant phases formed by surface decomposition after a high-temperature annealing, and another phase resulting from a lower-temperature annealing.

II. EXPERIMENTAL DESCRIPTION

The experiments were performed on surfaces of the ξ'-Al-Pd-Mn approximant crystals extracted from two different single grains. The first one was grown by the Bridgman method using a nominal composition of $Al_{77.5}Pd_{19}Mn_{3.5}$. The second one was grown by a self-flux technique starting from a ternary melt with a composition of $Al_{80.5}Pd_{17.25}Mn_{2.25}$.[16] The latter sample had a rodlike morphology, the pseudo-tenfold (p-10f) symmetry axis being the preferred growth direction. The composition of the resulting crystal as determined by energy dispersive x-ray spectroscopy (EDX) was approximately $Al_{72}Pd_{25}Mn_3$. Such crystals have dimensions up to 2 cm along the p-10f axis. Transmission electron microscopy (TEM) and x-ray diffraction were used to verify the crystal structure of both types of samples, and TEM was used to check for crystalline imperfections, especially phason strain.[17] Selected area diffraction patterns (SADP's) were obtained for the three diad axes [100], [010], and [001]. Lattice images were also obtained from some zones, principally the [010]. The flux-grown samples usually showed few phason defects and were mostly perfect ξ' phase, whereas the density of bulk defects was much higher in the Bridgman-grown samples. The lattice parameters determined from SADP's were $a_{\xi'}=23.4$ Å, $b_{\xi'}=16.5$ Å, and $c_{\xi'}=12.4$ Å, consistent with previously published values.[18] The high-energy electron-diffraction patterns were consistent with the *Pnma* space group expected for the ξ' phase.

Both samples were oriented by Laue to within $\pm 0.2°$ of the p-10f axis, and mechanically polished down to 0.25 μm. The size of the Bridgman-grown sample was fairly large (over 1 cm^2) and its chemical composition was homogeneous over the entire surface. *A contrario*, the flux-grown sample presented regions of nearly pure Al detected by scanning electron microscopy and EDX, coexisting with the ξ' phase, especially in the center of the sample, due to flux inclusions (and eutectic solidification). In spite of this inhomogeneity, the LEED pattern was uniform across the sample. This indicates that LEED did not sense the regions of Al-rich phase, except perhaps as a contribution to the background intensity. In the following, we will refer to the Bridgman-grown sample as BG and to the flux-grown sample as FG.

The QC sample was grown by the Bridgman method and its chemical composition was $Al_{72}Pd_{19.5}Mn_{8.5}$.[19] A surface perpendicular to the fivefold symmetry axis was extracted and polished in the same manner as previously described.[14] The samples were mounted on Ta plates and loaded into the UHV chamber that was equipped with an Omicron variable temperature STM and a LEED-Auger spectrometer. A clean surface was achieved by cycles of Ar^+ sputtering at room temperature followed by annealing. The Ar^+ beam energy was progressively reduced from 2 to 0.5 kV, and the etching time was about 30 min for each cycle. The typical annealing temperatures we used were 820 K for the ξ' approximant and 900 K for the icosahedral phase. The annealing time prior to a LEED or an STM experiment ranged from 2 to 4 h.

III. RESULTS

A. The ξ' approximant grown by the Bridgman method

The LEED pattern of the clean surface of the BG sample is shown in Fig. 1(a). It is dominated by two rings of bright diffraction spots with apparent tenfold symmetry. The ratio between the diameters of the two rings equals 1.6, consistent with the golden mean $\tau \sim 1.618$. More diffraction spots with faint intensity are also visible. All diffraction spots form lines that are periodically spaced, which is an essential difference from the diffraction pattern of the fivefold surface of the icosahedral QC shown in Fig. 1(b). Also, the diffraction spots forming the decagonal ring are of equal intensity in the case of the ξ' approximant, whereas two sets of five spots with different intensities can be distinguished in the case of the QC for the same energy.

STM examination of the BG sample surface after a few sputter-annealing cycles reveals a terrace and step morphology. This structure, which is found over the whole surface, displays several differences from the terrace and step structure usually associated with the quasicrystalline termination of the fivefold QC sample. First, the terraces are exceptionally large, sometimes bigger than 1 μm^2, as shown in Fig. 2(a). (While similar-sized terraces have been reported for the fivefold surface of a QC sample by another group,[6] we find that they are typically smaller.) Second, the step edges appear relatively smooth on the surface of the ξ' approximant, whereas step edges are usually irregular and meandering on the fivefold surface of the QC. Third, line profiles across the ξ' step edges reveal a single step height as expected for a periodic crystal. This is unlike the three step heights found on the quasiperiodic surface. Height histograms, such as that shown in Fig. 2(b), were used to determine the step height of the ξ' sample, $h=8.07$ Å (the root-mean-square value is $\sigma=0.16$ Å). (This approach is more accurate than using line profiles.) The measured value of h corresponds roughly to half the period ($b_{\xi'}=16.5$ Å) along the p-10f axis, which is the $\mathbf{b}_{\xi'}$ axis.

Further insight into the nature of the steps is provided by examining the ξ' structure model proposed by Boudard *et al.*,[18] which describes the unit cell as a stacking of flat and puckered layers along the p-10f axis. Only four different types of layers are identified. These fall at $y=0$, 0.12, 0.16, and 0.25 in units of $\mathbf{b}_{\xi'}$, the other layers in the unit cell being deduced from space-group symmetries. The four layers are reproduced in Fig. 3. The fact that the step height measured by STM corresponds to half of the period suggests that

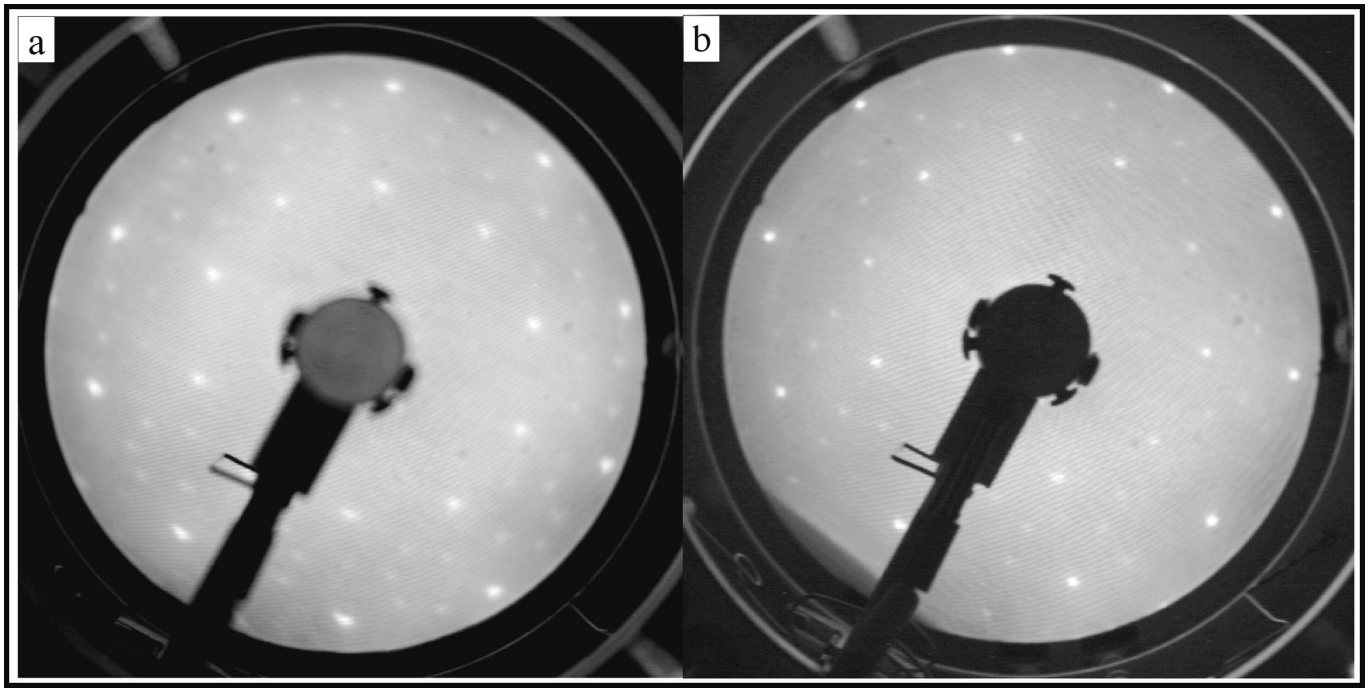

FIG. 1. LEED pattern at 85 eV of the Bridgman-grown (BG) ξ'-$Al_{77.5}Pd_{19}Mn_{3.5}$ sample in (a) and of the five-fold surface of the icosahedral $Al_{72}Pd_{19.5}Mn_{8.5}$ QC in (b).

the most favorable atomic layers for surface termination correspond to a particular pair of layers, which are related by a mirror plane.

Higher magnification in STM reveals a fine structure on the terraces, which can also be understood in light of the Boudard *et al.*[18] model. Figure 2(b) presents a $100 \times 100\ nm^2$ STM image recorded on one of the terraces. The inset includes a height histogram and the fast-Fourier transform (FFT) of this same image. The height histogram suggests that STM actually probes two different layers: the white dots correspond to groups of atoms that form an incomplete top layer atop a more dense (darker) bottom layer. In addition, line profiles in the darker regions of the image reveal that the bottom layer has an intrinsic corrugation of 0.7 Å (equal to the difference between the minimum and maximum of the line profiles). Also, line profiles across white dots show that they lie about 1.39 Å above the top of the bottom layer.

The interpretation of this fine structure is as follows. First, the 1.39 Å distance is only slightly shorter than the distance between the planes $y=0.16$ and $y=0.25$ of the bulk model, which is 1.49 Å. Second, the corrugation of the bottom layer itself (measured as 0.7 Å) corresponds to the distance between planes $y=0.12$ and $y=0.16$, which is 0.66 Å. Third, the plane at $y=0.16$ has a very low atomic density. We therefore postulate that the bottom layer seen in the STM image

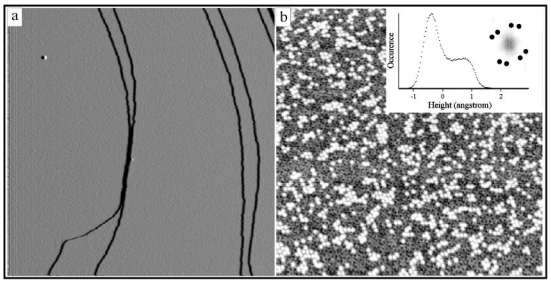

FIG. 2. a) STM image ($2\times2\ \mu m^2$) showing the terrace and step morphology of the p-10f surface of the (BG) ξ'-$Al_{77.5}Pd_{19}Mn_{3.5}$ approximant. b) STM image ($100\times100\ nm^2$) of the fine structure on a terrace. Inset: height histogram and FFT of the same image. The principal spots in the FFT have been enhanced for clarity, and appear as black dots.

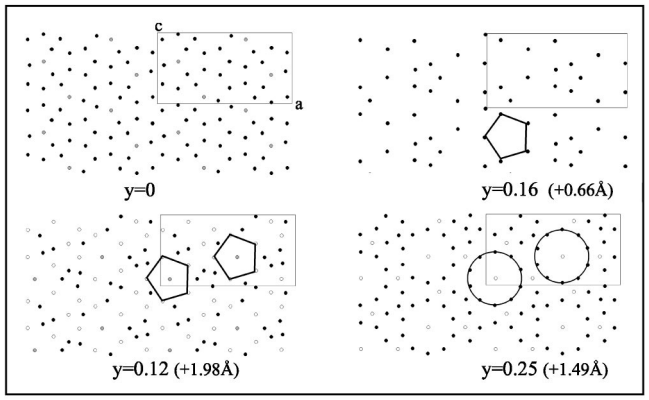

FIG. 3. The layer structure perpendicular to the $\mathbf{b}_{\xi'}$ axis of the ξ' phase according to the structure model by Boudard *et al.*[18] The four different layer types at $y=0$, 0.12, 0.16 and 0.25 in units of $\mathbf{b}_{\xi'}$ are represented. The distances between consecutive layers are mentioned in parenthesis. Black circles are Al atoms, white circles are Pd atoms, gray circles are Mn atoms. The unit cell in the ($\mathbf{a}_{\xi'}$,$\mathbf{c}_{\xi'}$) is outlined.

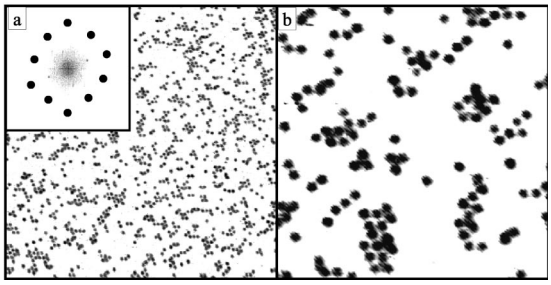

FIG. 4. a) Same as Fig. 2(b) but a ''height filter'' has been applied to select only the top layer. Inset: corresponding FFT. b) Enlarged view (30×30 nm^2) of the image in a) showing the regular size and morphology of the groups of atoms forming the top layer.

originates from both the $y=0.12$ and $y=0.16$ planes, and that the top layer corresponds to an incomplete version of the $y=0.25$ layer of the Boudard *et al.*[18] model.

Because of the multiple layer morphology of the terraces, which produces roughness, we could not succeed in obtaining atomic resolution images. Still, some fine structure can be observed in the bottom layer, and the FFT of the STM image (Fig. 2) shows ten spots describing a squeezed decagon emphasizing the p-10f symmetry of the surface.

Figure 4(a) shows the same STM image as in Fig. 2, but a ''height filter'' has been applied in order to select only the top layer, which remains as a nonuniform pattern of black dots. The inset is a schematic of the FFT of the filtered image, and it is still composed of ten spots describing a squeezed decagon. This implies that the positions of the dots are not random but ordered, with the p-10f rotational symmetry. The closer view in Fig. 4(b) shows that each dot has the same nearly circular geometry and a diameter of 10.03 Å ($\sigma=0.59$ Å). They must therefore correspond to groups of atoms forming a specific geometric motif. The closest distance between the centers of two adjacent groups is 12.3 Å ($\sigma=1.1$ Å).

The next step is to compare these observations concerning the top layer directly with the equivalent plane at $y=0.25$ of the bulk model. This plane is composed of Al decagonal rings surrounding a central Pd atom, outlined in Fig. 3.[18] The rings are located close to the vertices and the center of the rectangular 2D unit cell. The diameter of the decagons is 9.6 Å. The distance between centers of adjacent decagons is 12.5 Å. These values match reasonably well with our observations and we can therefore identify the groups of atoms forming the top layer observed in our STM image as these decagonal rings of Al atoms. In the bulk model, the rings are parts of 3D clusters of the Mackay type. The clusters are composed of a central Pd atom surrounded by a first icosahedral shell formed by Al (and Mn) atoms. A second shell is made of a larger icosahedron of Pd and an icosidodecahedron of Al. The clusters are connected by smaller and slightly distorted icosahedra. In the 2D plane at $y=0.25$, this 3D cluster structure results in decagonal rings interconnected by glue atoms forming slightly distorted pentagons. In our experiment, we observe that in the incomplete top layer, only the decagonal rings are restored after the sputter-annealing cleaning process. This suggests that the cluster sites are energetically more favorable than the glue sites, explaining why the decagonal rings—the black dots in Fig. 4—appear isolated from each other in the STM image.

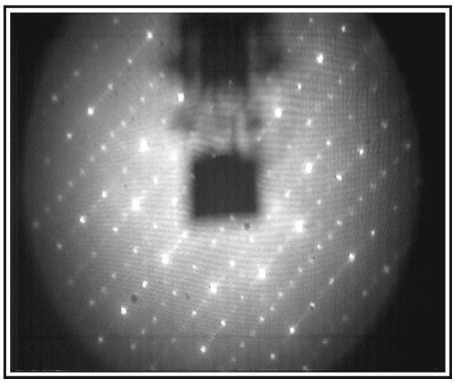

FIG. 5. LEED pattern at 75 eV of the p-10f surface of the ξ'-$Al_{72}Pd_{25}Mn_3$ approximant (FG sample).

B. The ξ' approximant grown by the self-flux technique

We now describe the surface structure of the FG sample. We mentioned already that this sample presents regions of an Al-rich phase detected by scanning electron microscopy and EDX, coexisting with regions where the chemical composition corresponds to the ξ' phase. This sample was first loaded into a UHV chamber dedicated to LEED experiments. The resulting diffraction pattern at 75 eV is shown in Fig. 5. Similar to the BG sample, the brightest spots comprise two rings, the ratio between the diameters of the two rings again being close to the golden mean, $\tau\sim1.618$. Furthermore, the positions of the diffraction spots in the LEED patterns of both samples are compatible with an orthorhombic crystal, and the spot intensities reflect the expected p-10f symmetry produced by the local icosahedral order of the structurally complex ξ' phase. But differences also exist between the two samples. First, more diffraction spots are visible in between the main p-10f rings for the FG sample than for the BG sample. This may be due to differences in short-term sample history (e.g., number of annealing cycles to which the sample had been subjected prior to LEED), or due to the coexistence of several phases contributing to the LEED pattern in the case of the FG sample. The higher intensity and abundance of these ''extra'' spots makes the diffraction pattern in Fig. 5 look more periodic than the diffraction pattern of the BG sample. We will argue later, in light of TEM results, that this is probably due to the higher density of bulk structural defects contained in the BG sample, leading to incommensurate structures that emphasize the aperiodic ''aspect'' of the pattern. The local probe of the STM also reveals clear differences between the surface structures of the BG and FG samples, as described in the remainder of this section.

After several sputter-annealing cycles, the FG surface was composed of flat regions with a terrace and step morphology, separated by very rough regions impossible to image with the STM. The flat regions themselves were of two different types. Figures 6 and 7 show the two different terrace-step

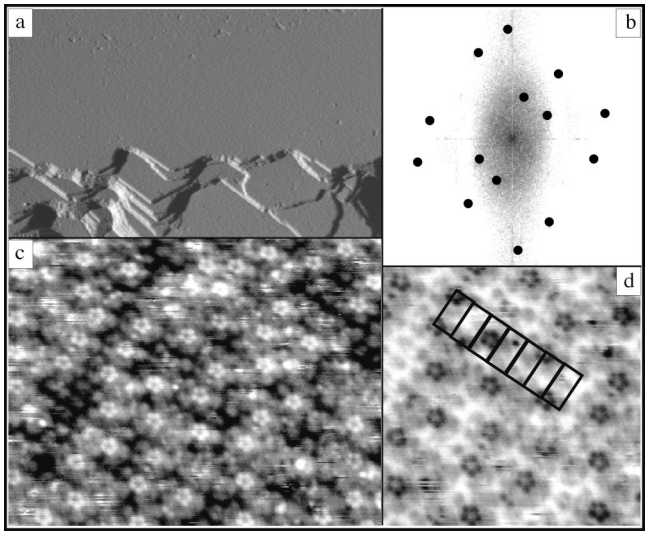

FIG. 6. STM images showing the first type of terraced morphology and fine structure observed on the surface of the flux-grown (FG) ξ'-$Al_{72}Pd_{25}Mn_3$ approximant. a) 500×300 nm^2; b) FFT, c) 70×48 nm^2; d) 17×17 nm^2. The principal spots in the FFT have been darkened for clarity.

structures. Each was encountered in homogeneous domains of the order of several microns in size. The tip had to be shifted by several tens of microns to change from one type of structure to the other. Therefore at least two different types of microstructures coexist on the surface of the FG sample.

We first describe the type of structure whose characteristics are shown in Fig. 6. The flat terraces are separated by straight step edges with a single step height of about 8 Å [Fig. 6(a)]. This value is similar to the step height measured for the BG sample, but the average terrace size is smaller and

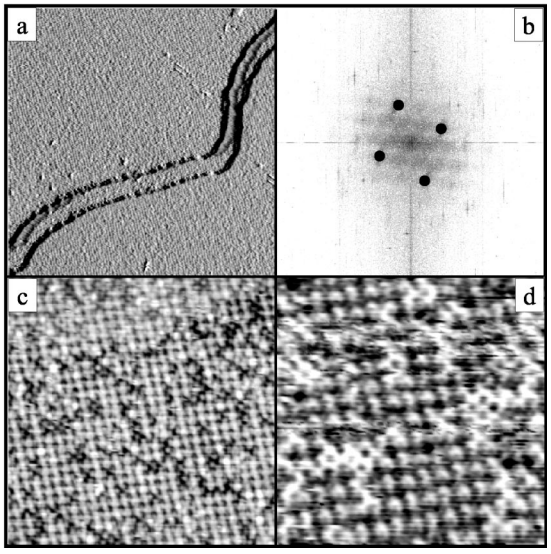

FIG. 7. STM images showing the second type of terraced morphology and fine structure observed on some regions at the surface of the flux-grown (FG) ξ'-$Al_{72}Pd_{25}Mn_3$ approximant. a) 200×200 nm^2; b) FFT; c) 50×50 nm^2; d) 30×30 nm^2. The principal spots in the FFT have been darkened for clarity.

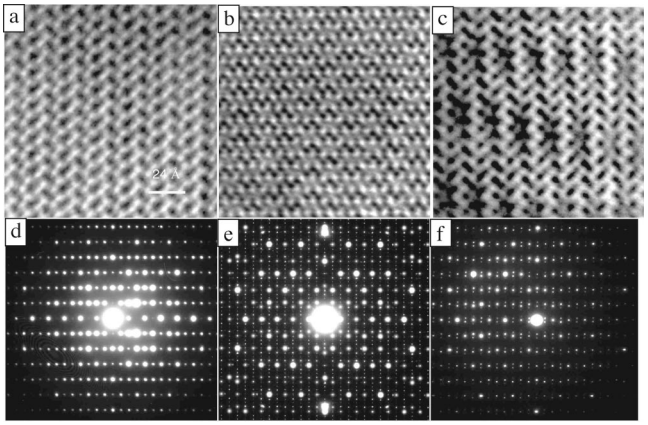

FIG. 8. HREM micrographs (top) and corresponding SADPs (bottom) along the p-$10f$ axis of the ξ' approximant (FG samples) containing various degree of disorder. The left column (*a,d*) corresponds to the perfect ξ' single crystal. The HREM image reveals the flattened hexagons arranged in zigzag. (*b,e*) and (*c,f*) correspond to two typical regions where phason-induced defects lead to new orderings.

the multiple layer morphology on a single terrace is not observed. The fine structure [Fig. 6(c)] is characterized by pentagonal motifs with bright contrast. A closer view is presented in Fig. 6(d), with a different contrast to enhance the pentagonal features. The pentagons are about 0.4 Å above the average height of the surface. The side of the pentagons is about 5.7 Å ($\sigma=0.26$ Å). This is deduced from the STM images by measuring the peak-to-peak distance between adjacent maxima in line profiles taken along the edges of the pentagons. Although the pentagonal features seem to be located at random, the surface is actually quite well ordered. This is shown by the FFT of the STM image, which is compatible with an orthorhombic lattice [a schematic of which is shown in Fig. 6(b)]. In addition, all the pentagons point in the same direction.

Here again, we can relate the pentagonal motifs observed experimentally to geometrical features in the different layers of the bulk model by Boudard *et al.*[18] Local pentagonal symmetry is found in each of the layers (see Fig. 3), but sufficiently large pentagons only appear at $y=0.12$ and $y=0.16$. Their edge length is equal to 4.89 Å. This is smaller by about 1 Å than the experimental value (5.7 Å), but is still within about 3σ associated with the lengths measured by STM. Noting that surface relaxation effects could also take place, we believe that both pentagons outlined in Fig. 3 are reasonable candidates. We must now decide which of these two is the most consistent with our observations. According to the bulk model, the pentagons at $y=0.12$ are made of one Mn central atom surrounded by five Pd atoms. This layer is dense and puckered, the atomic positions actually lying in a range $0.08\leqslant y\leqslant0.12$. The Pd atoms are about 0.6 Å above the central Mn atom and about 0.3 Å above the average height of the surface, consistent with the values reported above. The pentagons at $y=0.16$ are made of five Al atoms and there is no central atom. As mentioned above in the analysis of the BG sample surface, this layer has a very low atomic density such that the STM tip should also probe the

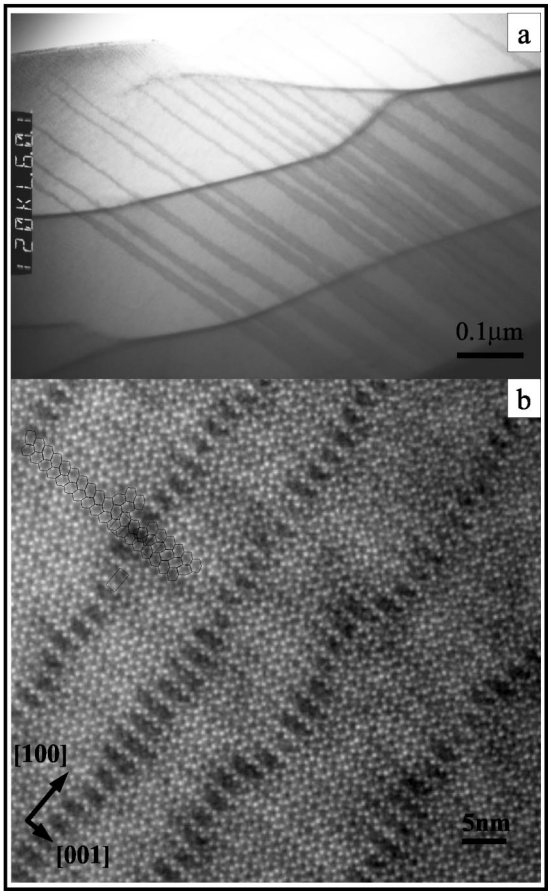

FIG. 9. HREM micrographs taken perpendicular to the p-10f axis of the ξ' approximant (FG sample). a) low magnification image showing terraces crossed by linear defects. b) higher magnification showing the arrangement of the flattened hexagons arranged in zigzag. In the region of linear defects (darker regions), the order is altered. The scale is given by the rectangular unit cell drawn on the image.

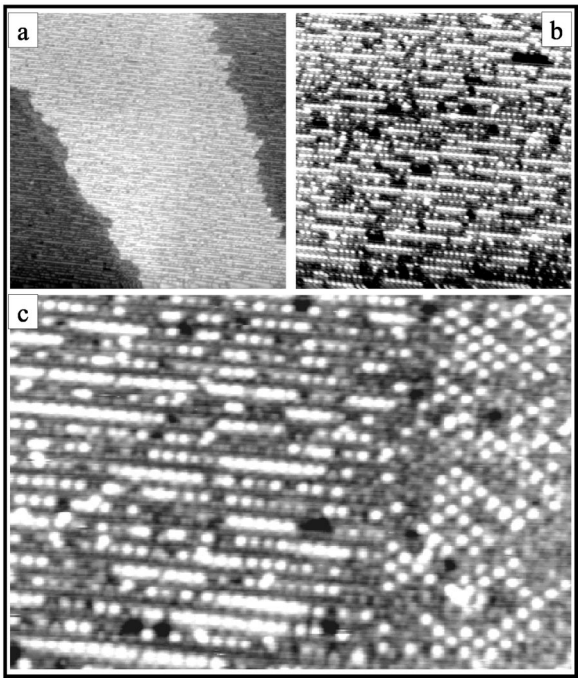

FIG. 10. a-c) STM images obtained on the five-fold icosahedral QC surface after decomposition by annealing at low temperature. a) 150×150 nm^2; b) 50×50 nm^2; c) 40×26 nm^2.

next layer at $y=0.12$. If this were the case, then the corrugation of the terraces would be larger than that observed experimentally. Also, adjacent pentagons connected by vertices are present in the layer at $y=0.16$ but not in the STM images. These arguments suggest that the layers at $y=0.12$ are favorable atomic planes for surface termination in the case of the FG sample. Then the bright features with pentagonal symmetry are identified as small rings made of five Pd atoms on top of a central Mn atom.

For the BG sample, the bright features seen in the STM images were identified as Al decagonal rings that are cross sections, at $y=0.25$, of the bulk Mackay-type clusters of the model of Boudard *et al.* For the FG sample, the motifs of bright contrast with fivefold symmetry are identified as Pd pentagonal rings that are also cross sections, at $y=0.12$, of the *same* clusters. In the surface plane perpendicular to the $[010]_{\xi'}$ axis, the cross sections of these clusters are located at the nodes and at the center of the rectangular unit cell. Accordingly, if the surface structure, like the one shown in Fig. 6, was a perfect truncation of the bulk along the $y=0.12$ layer, then the set of bright pentagonal motifs should form a perfect rectangular centered lattice, which is not observed. However, the positions of the pentagons in the STM images are consistent with this scheme. For example, it is possible to superimpose a set of unit cells on the STM image, from which we see [Fig. 6(d)] that the pentagonal rings are located either at the nodes or at the center of the rectangular lattice. These sites appears to be either occupied by a complete pentagonal ring or they are completely vacant.

This fact—that the pentagonal rings are either completely present or completely absent—again suggests that rebuilding

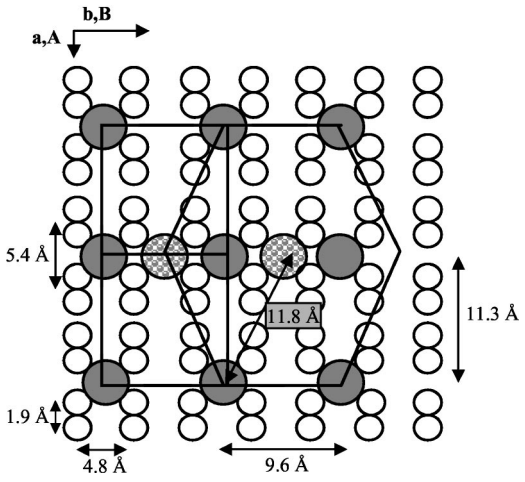

FIG. 11. Proposed structural model deduced from STM images as in Fig. 9. The large gray circles correspond to the brightest features in the STM pictures. The white circles correspond to the smaller features in the STM image which form the underlying lattice (see text). Distances are deduced from line profiles taken along and across the direction defined by the rows of bright spots.

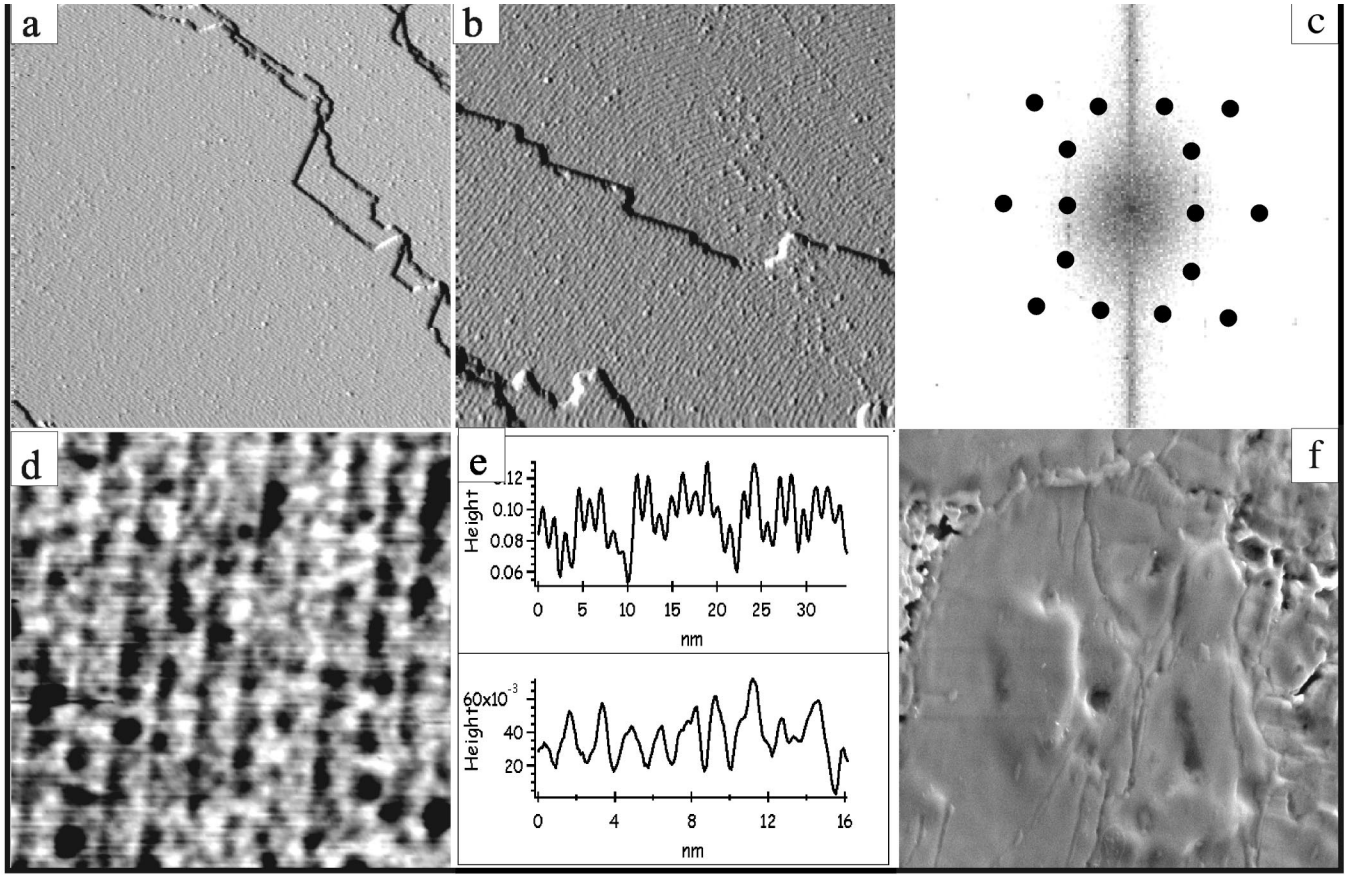

FIG. 12. a-d) STM images showing the terraced morphology and some fine structure for the *T*-approximant of Al-Pd-Mn. a) 150 $\times 150$ nm^2; b) 100×100 nm^2; c) FFT; d) 15×15 nm^2. e) height profiles across (top) and along (bottom) the lines of bright contrast. f) SEM image (8.5×8.5 μm^2). The principal spots in the FFT have been darkened for clarity.

the Mackay clusters after the sputter annealing is a common tendency on the p-10f surface of the ξ' crystals. In summary, although the surfaces of the BG and the FG samples terminate at different layers, both surfaces share a common feature, which is that the cluster sites seem energetically favored as compared to the glue sites.

The characteristics of the second type of terrace-step structure encountered on the surface of the FG sample are shown in Fig. 7. Again, we find flat terraces with a roughness smaller than 0.6 Å separated by step edges, but here several step heights are measured, which are all equal to an integer number of $h\sim 2$ Å. The FFT of the STM image in Fig. 7(b) suggests a square lattice. This is confirmed by the fine structure on the terraces shown in Figs. 7(c) and 7(d). The dimensions of the 2D unit cell in the plane of the surface can be deduced from the STM image and is about 19×19 Å^2. The square lattice contains some structural defects. To the best of our knowledge, the lattice parameters as deduced from our data do not correspond to any identified approximant of the QC phase.

The results presented above revealed differences between the BG and the FG samples at their surfaces. Also the FG sample seems to contain an extra phase. To gain insight into the possible origin of these differences, a TEM study on both types of samples was undertaken. Approximant structures formed in this region of the phase diagram have already been studied by TEM.[17,18,20] In particular, Klein *et al.* showed that the ξ' phase was related to another ξ approximant by a phase transformation occurring through plastic deformations.[17] Another approximant phase named ξ'' and containing structural defects (phason defects) was also observed by TEM and interpreted as an intermediate state of such a phase transformation.

Figure 8 shows some examples of high-resolution electron microscopy (HREM) micrographs and their corresponding SADP's viewed along the p-10f axis for a FG sample (left column) and a BG sample (central and right columns). These samples were extracted from the same ingots as the particular samples used in the surface study. The FG sample appears as a mostly perfect ξ' phase [Fig. 8(a)], although some limited regions contained linear defects. Evidence for a much higher density of defects is found for the BG samples [Figs. 8(b) and 8(c)].

Finally, because two different types of structure were observed on the FG sample by STM, this particular sample was further analyzed by TEM after the STM experiments, to check whether the bulk structure had remained intact. A thin slice was cut perpendicular to the p-10f axis and mechanically thinned, then dimpled and ion milled. The typical SADP pattern taken along the $[010]_{\xi'}$ direction confirms that the sample is, in general, still a good ξ' single crystal with

large defect-free areas. Some spots corresponding to a thin $B2$ cubic layer with a lattice parameter equal to 3.15 Å are also present in the diffraction pattern. Another type of diffraction pattern was observed less frequently, which corresponds to a 1D-incommensurate modulated structure based on the ξ' lattice. The parameters of the modulated lattice are ($a_{\mathrm{mod}}=a_{\xi'}=23.4$ Å and $c_{\mathrm{mod}}=6.81c_{\xi'}=87.8$ Å). The HREM image at low magnification in Fig. 9(a) shows the presence of terraces crossed by linear defects. The density of defects is rather low over most of the sample but can be high in some limited areas, like the one shown in Fig. 9(a). Figure 9(b) is a higher magnification of a typical region crossed by linear defects. The packing of the flattened hexagonal units arranged in zigzag, which is characteristic of the ξ' phase, can be observed. In the region of linear defects, the phase of the hexagons is altered. The defects develop along the $[100]_{\xi'}$ direction because the defect structure has the same periodicity ($a_{\mathrm{mod}}=a_{\xi'}$). The growth along the $[001]_{\xi'}$ direction is quite limited because of the incommensurability ($c_{\mathrm{mod}}=6.81c_{\xi'}$).

These observations by TEM shed some light on the STM results presented earlier. First, the square lattice with parameter ~19 Å deduced from the STM images (Fig. 7) could be related in some way to the thin $B2$ cubic layer with parameter ~3.15 Å seen in the SADP's. The formation of the cubic layer could result from the ion milling used to prepare the sample for TEM. It could also have been formed during the surface preparation process in the STM chamber. Indeed, the formation of a metastable $B2$ overlayer on the high-symmetry surfaces of the icosahedral Al-Pd-Mn QC is a frequent phenomenon.[21] For the fivefold surface, the orientation relationship corresponds to the $[110]_{B2}$ axis parallel to the fivefold axis of the underlying QC.[22] In the present case, the $[110]_{B2}$ axis would be parallel to the p-10f $[010]_{\xi'}$ axis. Then, perpendicular to the surface plane, the distance between (110) consecutive planes (i.e., the step height) should be about $3.15/\sqrt{2}=2.2$ Å, which is consistent with the experimental step heights being integral multiples of about 2 Å. In the (110) surface plane, the unit cell should be a rectangle with edge lengths equal to 3.15 and $3.15\sqrt{2}=4.5$ Å. Then the ratio between the parameters of the square lattice (19 Å) and of the rectangular $(110)_{B2}$ lattice are close to integral values ($19/3.15\sim6$, $19/4.5\sim4$), suggesting that the surface structure in Fig. 7 could be a (6×4) superstructure on the $(110)_{B2}$ surface. This hypothesis is supported by a previous LEED study of a single-grain sample of this material, which showed several reconstructions of the (110) surface.[22]

Finally, the TEM analysis shows that the main difference between the BG and the FG single crystals is the density of bulk structural defects that they contain, with the BG sample containing a higher defect density. The STM images shown in Figs. 2 and 6 both correspond to the ξ' phase or a disordered version of it. At present there are insufficient data to correlate the various types of surface terminations observed by STM to the degree of structural quality of the bulk structures as observed by TEM. However, the high density of linear defects corresponding to 1D-incommensurate modulated structures in the BG samples could account for the differences noted above between the LEED patterns of both samples. In general, our work demonstrates the variability of results that can be obtained when studying surfaces of samples that nominally belong to the same bulk phase in such complex materials.

C. Other crystalline phases induced by sputter annealing on the fivefold surface of an $Al_{72}Pd_{19.5}Mn_{8.5}$ icosahedral quasicrystal

We now turn to a description of several periodic structures that appeared as overlayers on the fivefold surface of an $Al_{72}Pd_{19.5}Mn_{8.5}$ icosahedral QC sample after specific annealing conditions.

The first one was observed in the central part of the QC sample surface after annealing at a relatively low temperature (770 K), while regions closer to the edges of the sample presented the usual characteristics of the fivefold quasiperiodic surface. We mention that the sample surface had a lusterless appearance after the annealing, which is unusual as it normally retains the mirrorlike finish given by the mechanical polishing.

STM images of this ''low-temperature'' phase are shown in Fig. 10. Terraces are separated by steps that are 1.9 ± 0.1 Å high. Incomplete rows of bright spots appear on the terraces that look, therefore, anisotropic. The diameter of a bright spot is about 7 Å ($\sigma=0.40$ Å). The distance between two adjacent rows is $A=11.3$ Å ($\sigma=0.73$ Å). Along the rows, the distance between two adjacent bright spots is $B=9.6$ Å ($\sigma=0.22$ Å). In areas where the bright spots are missing, the STM can resolve additional smaller features. Line profiles taken either along or perpendicular to the direction of the rows leads to the structural model proposed in Fig. 11. In that scheme, the underlying lattice would be rectangular with parameters $a=1.9$ Å and $b=4.8$ Å. Then the bright dots would form a rectangular lattice identified as a $p(6\times2)$ reconstruction on the underlying lattice. The positions along the **B** direction tend to be more frequently occupied than the positions along the **A** direction, explaining the apparent anisotropy on the STM images.

Note that on the right side of the STM image in Fig. 10(c), the lattice formed by the bright dots looks hexagonal rather than rectangular. This was observed in limited areas of the sample surface. The occurrence of this hexagonal structure can be understood using the same structural model as in Fig. 11. Indeed, the transformation from the rectangular to the hexagonal lattice only requires that one row of bright dots out of every two be shifted by the translation vector **B**/2. This is illustrated schematically in Fig. 11. If this interpretation is correct, the edge length of each hexagon formed by the bright dots should equal $\sqrt{A^2+(B/2)^2}=12.2$ Å, which is very close to the value of 11.8 Å ($\sigma=0.56$ Å) measured from the STM images. At present we cannot identify this structure further; its characteristics do not correspond to a known bulk phase.

Finally, we describe the surface of another type of approximant structure that appeared after annealing the fivefold surface of an $Al_{72}Pd_{19.5}Mn_{8.5}$ icosahedral QC at a higher temperature (920 K). After the heat treatment, the surface had also a dull, lusterless appearance. This sample was actually

extracted from the same ingot as the sample used above. We believe that the surface transformation described below is similar to previous observations by Ledieu *et al.*[23]

Flat areas with a terrace and step morphology could be observed with a μm size, separated by rough regions impossible to image with the STM. Figure 12 is a montage of STM images of terraces and their fine structure. The step edges are straight, forming segments that are sometimes perpendicular to each other. The single step height equals 6.2 Å. As for the ξ, approximant (BG sample), we observed consistently, across several STM images, that a small terrace is usually followed by a larger one. Lines of bright contrast can be seen in Figs. 12(a) and 12(b), and a closer view is shown in Fig. 12(d). Atomic resolution could not be achieved but the FFT of one such image possesses symmetry compatible with an orthorhombic lattice. Furthermore, the height profiles in Fig. 12(e), taken parallel and perpendicular to these lines, show a periodicity in both directions, with a period equal to 15 and 13 Å, respectively. These values match very well with the lattice parameters of the T-$Al_{72/3}Pd_{3.2}Mn_{24.5}$ approximant, a_T=14.72 Å, b_T=12.51 Å, c_T=12.59 Å, as described by Klein *et al.*[24] Its structure can be described as the stacking of three different layers along the $\mathbf{b}_T$ p-10f symmetry axis. It seems natural to expect that the $\mathbf{b}_T$ axis would parallel the fivefold axis of the underlying quasicrystal and therefore the surface plane would correspond to the ($\mathbf{a}_T$,$\mathbf{c}_T$) plane. Then the experimental step height roughly equals half the value of the $\mathbf{b}_T$parameter. We speculate that the most favorable atomic plane for surface termination also corresponds to a particular pair of layers related by a mirror plane, just as in the ξ' phase.

After the STM experiment, the sample was removed from the chamber and loaded in another UHV chamber equipped with a scanning Auger microscope (SAM) and a scanning electron microscope (SEM). The surface had to be exposed to air during the transfer and therefore it was covered by an oxide layer. This surface as seen by SEM [see Fig. 12(f)] is made of plain and smooth areas coexisting with some other rough and porous regions. The surface composition give by Auger spectroscopy is $Al_{74}Pd_3Mn_{23}$, but this includes the contribution of the oxide layer to the Auger signal. After Ar^+ sputtering to remove the air contamination, the composition is $Al_{52}Pd_{13}Mn_{35}$ in the flat areas and $Al_{52}Pd_{22}Mn_{26}$ in the rough regions. These chemical compositions are derived using elemental sensitivity factors and are especially low in Al due to the well-known preferential sputtering effect in this system. It was not possible to anneal the sample in this UHV chamber. Nevertheless, the data show that the surface has decomposed into two phases, one of which is Mn rich and rather flat. The Mn enrichment is consistent with the hypothesis that part of the surface of the QC sample has transformed into the *T* approximant.

The Mn enrichment of the surface during the sputter-annealing cleaning process was observed on several samples issued from the same ingot. One of these samples was analyzed after the surface decomposition by EDX, along the sample thickness (perpendicular to the surface plane). It was found that the chemical composition was exactly that of the icosahedral phase, and no second phase could be detected. Noting that the spatial resolution of EDX is about 1 μm, and hence is unable to resolve the surface from the bulk along the surface normal, this result implies that the precipitation of second phase occurs only in the near-surface region. Finally, this sample was post-annealed in a sealed evacuated tube at 970 K for 7 days. It was then repolished down to 0.25 μm and loaded again in the STM chamber. No surface decomposition was observed for annealing temperatures up to 920 K, which is 20° higher than the annealing temperature we use to obtain the perfect quasicrystalline surface.[13] We suggest that this type of surface transformation, which has been reported by a few other groups[23,25] is not only determined by the annealing temperature but also by the long-term thermal history of the sample.

In summary, the Mn enrichment of the surface, the lattice parameters deduced from the STM images, and the FFT's compatibility with an orthorhombic lattice, all suggest that the complex crystalline phase formed by decomposition at high temperature corresponds to the *T* approximant. Our other observations suggest that a combination of the immediate and long-term thermal histories of the sample determine whether it will form. When it does form, it nucleates first at the sample's surface.

IV. CONCLUSIONS

We have observed the surface structure of several complex crystalline phases related to the icosahedral Al-Pd-Mn quasicrystal. Some of them appear as overlayers induced by sputtering and annealing on the five-fold QC surface. This includes the Mn-rich *T* approximant as well as a reconstructed surface probably corresponding to another complex orthorhombic phase. In these cases, the chemical composition in the near-surface region was driven out of the stability range of the icosahedral phase. The temperature at which the composition change occurred seems to depend on the sample's thermal history.

We also have presented results on the different mosphologies observed on the p-10f surface of ξ' single crystals, grown either by Bridgman or by a self-flux technique. For both samples, the LEED pattern shows the expected p-10f symmetry. Under the local probe of STM, the surface of the BG sample appears homogeneous but the FG contains one extra phase. The latter has a nearly square lattice with parameters that do not match any known approximant structure in this system, but could be related to the formation of a cubic B2 layer oriented with the $[110]_{B2}$ axis parallel to the p-10f axis of the ξ' crystal. This difference in phase purity, plus other differences in details of the LEED and STM data for the two samples, illustrates the variability that can arise in surface of samples derived from the same bulk phase, especially in such complex materials.

In spite of the differences, for both the BG and the FG samples, we have seen that details of the STM images can be identified as specific planes perpendicular t the p-10f axis of the bulk structure model derived by Boudard *et al.*[18] Just as for the fivefold QC, the surface obtained after sputter-annealing can thus be interpreted as arising directly from the ξ' bulk model. In particular, the incomplete top layer seen in

the high-resolution STM images actually corresponds to the preferential re-growth of decagonal rings (BG sample) or pentagonal motifs (FG sample) of atoms that are part of the same 3D cluster units of the ξ' phase. This is in contrast with the fivefold QC where the surface regrowth encompasses not only the cluster sites but also the ''glue sites,'' forming together a relatively dense and flat top layer.

This leads us back to the question raised in the Introduction about the relative stability of the cluster units. As reported in Ref. 18, the atomic structure of the ξ' shows a close local similarity with the icosahedral phase, and in particular they share similar cluster units. The fact that the cluster sites seem energetically more favorable than the glue sites for the approximant but not for the QC surface then suggests that the relative stability of the clusters not only depends on the clusters themselves but also on their environment, i.e., on the glue atoms.

ACKNOWLEDGMENTS

This work was supported by the Director, Office of Science, Office of Basic Energy Science, Materials Science Division of the U. S. Department of Energy under Contract No. W-405-Eng-82.

*Present address: LSG2M, CNRS-UMR 7584, Parc de Saurupt, F-54042 Nancy, France.

†On leave from Dalian University of Technology, 116024 Dalian, China.

**Present address: Geballe Laboratory for Advanced Materials and Department of Applied Physics, McCullough Bldg. Rm 359, Stanford University, CA 94305-4045, USA.

‡Corresponding author: thiel@ameslab.gov

[1] D. Shechtman, I. Blech, D. Gratias, and J. W. Cahn, Phys. Rev. Lett. **53**, 1951 (1984).

[2] A. P. Tsai, in *Physical Properties of Quasicrystals*, edited by Z. M. Stadnik, Springer Ser. Solid-State Sci. **Vol. 126**, pp. 5–50 (1999).

[3] M. Boudard, M. De Boissieu, C. Janot, G. Heger, C. Beeli, H. U. Nissen, H. Vincent, R. Ibberson, M. Audier, and J. M. Dubois, J. Phys.: Condens. Matter **4**, 10149 (1992).

[4] A. P. Tsai, in *New Horizons in Quasicrystals: Research and Applications*, edited by A. I. Goldman, D. J. Sordelct, P. A. Thiel, and J. M. Dubois (World Scientific, Singapore, 1997), pp. 1–8.

[5] M. Boudard, in *Quasicrystals: Current Topics*, edited by E. Belin-Ferré, C. Berger, M. Quiquandon, and A. Sadoc (World Scientific, Singapore, 2000), pp. 73–90.

[6] R. McGrath, J. Ledieu, E. J. Cox, and R. D. Diehl, J. Phys.: Condens. Matter **14**, R119–R144 (2002).

[7] J.-M. Dubois, J. Phys.: Condens. Matter **13**, 7753–7762 (2001).

[8] P. A. Thiel, A. I. Goldman, and C. J. Jenks, in *Physical Properties of Quasicrystals*, edited by Z. M. Stadnik, Springer Ser. Solid-State Sci. **Vol. 126**, pp. 327–359, (1999).

[9] P. Ebert, M. Feuerbacher, N. Tamura, M. Wollgarten, and K. Urban, Phys. Rev. Lett. **77**, 3827 (1996).

[10] L. Barbier, D. Le Floc'h, Y. Calvayrac, and D. Gratias, Phys. Rev. Lett. **88**, 085506 (2002).

[11] Z. Shen, C. R. Stoldt, C. J. Jenks, T. A. Lograsso, and P. A. Thiel, Phys. Rev. B **60**, 14 688 (1999).

[12] J. Ledieu, R. McGrath, R. D. Diehl, T. A. Lograsso, D. W. Delaney, Z. Papadopolos, and G. Kasner, Surf. Sci. Lett. **492**, L729 (2001).

[13] V. Fournée, T. Cai, A. R. Ross, T. A. Lograsso, J. W. Evans, and P. A. Thiel (in preparation).

[14] C. J. Jenks, D. W. Delaney, T. E. Bloomer, S. L. Chang, T. A. Lograsso, Z. Shen, C. M. Zhang, and P. A. Thiel, Appl. Surf. Sci. **103**, 485 (1996).

[15] M. Audier, M. Durand-Charre, and M. De Boissieu, Philos. Mag. B **68**, 607 (1993).

[16] I. R. Fisher, M. J. Kramer, Z. Islam, T. A. Wiener, A. Kracher, A. R. Ross, T. A. Lograsso, A. I. Goldman, and P. C. Canfield, Mater. Sci. Eng., A **A294–296**, 10–16 (2000).

[17] H. Klein, M. Audier, M. Boudard, M. De Boissieu, L. Beraha, and M. Duneau, Philos. Mag. A **73**, 309 (1996).

[18] M. Boudard, H. Klein, M. de Boissieu, and M. Audier, Philos. Mag. A **74**, 939 (1996).

[19] D. W. Delaney, T. E. Bloomer, and T. A. Lograsso, in *New Horizons in Quasicrystals: Research and Applications*, edited by A. I. Goldman, D. J. Sordelet, P. A. Thiel, and J. M. Dubois (World Scientific, Singapore, 1997), pp. 45–52.

[20] L. Beraha, M. Duneau, H. Klein, and M. Audier, in *Proceedings of the 6th International Conference on Quasicrystals*, edited by S. Takeuchi and T. Fujiwara (World Scientific, Singapore, 1998), pp. 207–210.

[21] Z. Shen, M. J. Kramer, C. J. Jenks, A. I. Goldman, T. Lograsso, D. Delaney, M. Heinzig, W. Raberg, and P. A. Thiel, Phys. Rev. B **58**, 9961 (1998).

[22] M. W. Heinzig, O. L. Warren, Z. Shen, C. J. Jenks, T. A. Lograsso, and P. A. Thiel, in Mater. Res. Soc. Symp. Proc. edited by J. M. Dubois, P. A. Thiel, A.-P. Tsai and K. Urban (Material Research Society, Warrendale, Pennsylvania, 1999, Vol. **553**), pp. 251–256.

[23] J. Ledieu, C. A. Muryn, G. Thornton, G. Cappello, J. Chevrier, R. D. Diehl, T. A. Lograsso, D. Delaney, and R. McGrath, Mater. Sci. Eng., A **A294–296**, 871–873 (2000).

[24] H. Klein, M. Boudard, M. Audier, M. De Boissieu, H. Vincent, L. Beraha, and M. Duneau, Philos. Mag. Lett. **75**, 197 (1997).

[25] D. Naumovic, P. Aebi, C. Beeli, and L. Schlapbach, Surf. Sci. **433–435**, 302 (1999).